Applied Catalysis B: Environmental 154–155 (2014) 197–205

Contents lists available at ScienceDirect

Applied Catalysis B: Environmental

journal homepage: www.elsevier.com/locate/apcatb

Development of a membrane electrode assembly for alkaline water electrolysis by direct electrodeposition of nickel on carbon papers

Sang Hyun Ahn[a], Byung-Seok Lee[a], Insoo Choi[a], Sung Jong Yoo[a], Hyoung-Juhn Kim[a], EunAe Cho[a], Dirk Henkensmeier[a], Suk Woo Nam[a], Soo-Kil Kim[b,*], Jong Hyun Jang[a,**]

[a] Fuel Cell Research Center, Korea Institute of Science and Technology (KIST), Hwarangno 14-gil 5, Seongbuk-gu, Seoul 136-791, Republic of Korea
[b] School of Integrative Engineering, Chung-Ang University, Heukseokno 84, Dongjak-gu, Seoul 156-756, Republic of Korea

ARTICLE INFO

Article history:
Received 30 November 2013
Received in revised form 29 January 2014
Accepted 11 February 2014
Available online 20 February 2014

Keywords:
Alkaline water electrolysis
Membrane electrode assembly
Hydrogen and oxygen evolution reactions
Electrodeposited Ni catalyst

ABSTRACT

A membrane electrode assembly (MEA) for use in an alkaline water electrolyzer is fabricated by sandwiching an anion exchange membrane (AEM) between two electrodes prepared by the electrodeposition of Ni (used as a catalyst) on carbon papers (CPs) acting as gas diffusion layers. The conditions for Ni electrodepositon are determined on the basis of the results of half-cell tests for hydrogen and oxygen evolution reactions. An MEA fabricated by the direct electrodeposition of an extremely low Ni amount of 8.5 $\mu g_{Ni}\,cm^{-2}$ exhibits a high cell performance of 150 $mA\,cm^{-2}$ at 1.9 V when a 1.0 M KOH solution is supplied to the cathode. Electrodeposited Ni is uniformly distributed on the surface of CP fibers, thereby providing a large electrochemical surface area for gas evolution reactions and thus maintaining high catalyst utilization. It is suggested that control of bubble generation and AEMs with higher ionic conductivity would further increase MEA performance.

1. Introduction

In recent years, hydrogen has been recognized as an alternative energy source to mitigate global climate changes [1,2]. To establish a hydrogen-based economy, hydrogen production using water electrolyzers associated with renewable energies (*e.g.*, solar, wind and tidal energies) should be preferentially considered because it is an environmental friendly process with zero emission of greenhouse gases [3,4]. For several decades, alkaline water electrolyzers (AWEs) have been investigated to produce hydrogen from water on a large scale [5]. When electrolysis is carried out at high pH values, non-noble metals (*e.g.*, Ni, Co, and Mo) can be used as catalysts, thereby providing cost effectiveness [6]. However, when an alkaline solution with a porous diaphragm is used as the electrolyte, the generated oxygen (at the anode) and hydrogen (at the cathode) gases can easily crossover, thereby decreasing the purity of the produced hydrogen, and a large gap between the two electrodes can increase ohmic resistance [7]. In addition, the gas crossover through the diaphragm also prevents rapid startup/shutdown [7].

On the other hand, a proton exchange membrane water electrolyzer (PEMWE), which utilizes solid electrolytes with high proton conductivity, can overcome the drawbacks originating from the use of a diaphragm; that is, it can largely reduce the ohmic voltage drops and gas crossovers. As a result, the hydrogen production rate, energy efficiency, and hydrogen purity can be enhanced, as well as a more rapid startup/shutdown operation can be realized [8,9]. In the last decade, with large technical advancements made in the field of proton conducting membrane materials, many research groups have focused on the development of PEMWEs [10,11]. However, because of the highly acidic environment in PEMWEs, noble metals and their oxides (*e.g.*, Pt, Ir, Ru, IrO_2, and RuO_2) must be used as electrocatalysts for both hydrogen evolution reactions (HERs) and oxygen evolution reactions (OERs). This requirement poses a hindrance to the commercialization of PEMWEs in the form of high material costs [12,13].

More recently, alkaline anion exchange membrane water electrolyzers (AAEMWEs), in which an AEM is used as an electrolyte membrane, are receiving great attention [14–24] owing to their several advantages: use of non-noble metals as catalysts, low ohmic resistance, and good gas separation characteristics of solid membrane electrolytes. However, for practical applications, the conductivity and stability of a hydroxide ion conducting polymer membrane should be further enhanced; in fact, many research groups are actively working on specific candidate materials

* Corresponding author. Tel.: +82 2 820 5770; fax: +82 2 814 2651.
** Corresponding author. Tel.: +82 2 958 5287; fax: +82 2 958 5199.
E-mail addresses: sookilkim@cau.ac.kr (S.-K. Kim), jhjang@kist.re.kr, jonghyun.jang@gmail.com (J.H. Jang).

http://dx.doi.org/10.1016/j.apcatb.2014.02.021
0926-3373/

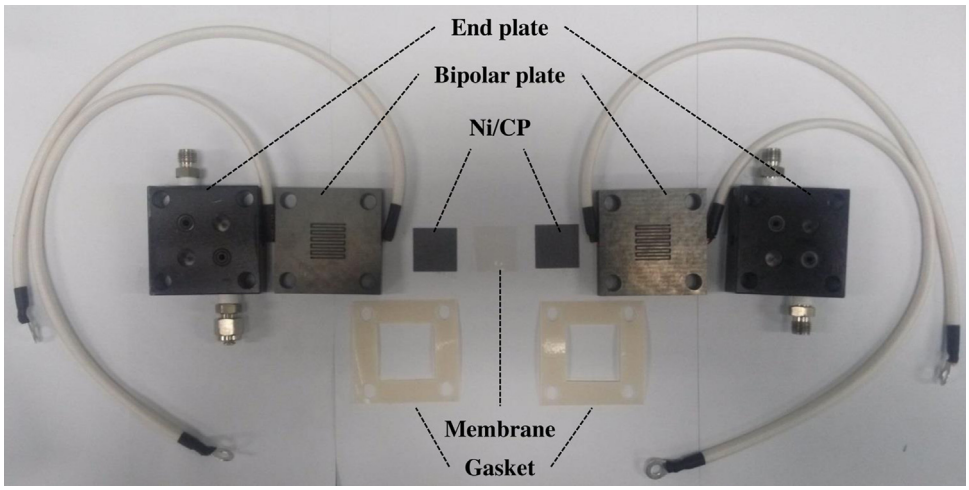

Fig. 1. Photograph of AAEMWE cell configuration.

[25–29]. In addition, the development of novel catalysts and electrodes is required for reducing material costs; however, compared to PEMWEs, relatively less research has been conducted in this field. Typically, large amounts of catalysts are loaded with anion-conducting ionomers to form thick catalyst layers on both sides of an AEM. For example, Wang et al. prepared a catalyst-coated membrane (CCM) by using Pt (3.2 mg cm^{-2}) and IrO_2 (2.9 mg cm^{-2}) for fabricating the cathode and anode, respectively [14]. Recently, Co- and Cu-based OER electrocatalysts [15–20] and Ni-alloy catalysts [21,22] have been developed to replace expensive Pt- and Ir-based catalysts; however, catalyst loading is still maintained at a high level of ~3 mg cm^{-2}. Ni bulk materials such as foams [23] and plates [24] have also been utilized as AAEMWE electrodes, but these materials are also plagued by problems such as high material costs due to the use of large amounts of metal catalysts.

In this study, extremely low amounts of Ni (used as a catalyst; 8.5 μg_{Ni} cm^{-2}) were directly deposited on carbon papers (CPs) by electrodeposition and the fabricated Ni/CP electrodes were utilized both as a cathode (HER) and an anode (OER) to construct a highly efficient AAEMWE. The effect of electrodeposition voltage and time was investigated in order to achieve high catalytic activity of Ni/CP electrodes toward HER and OER. Then the AAEMWE single cell performances were evaluated at various MEA compression pressures and operating temperatures. Since the fabricated electrodes were very thin, water (a reactant) and generated gases were expected to be transported rapidly [30].

2. Experimental

The electrolyte used in Ni electrodeposition was prepared using a metal precursor (0.50 M $NiCl_2 \cdot 6H_2O$, Kanto Chemical Co.), a pH adjustor (pH = 2.5, HCl, Sigma–Aldrich), and deionized water [31]. Ni electrodeposition was performed using a conventional three-electrode cell. A CP without polytetrafluoroethylene (TGPH-090, Toray) was used as a working electrode for enhancing the wettability toward the electrolyte. The geometrical area of the working electrode exposed to the electrolyte was 10.24 cm^2, and other parts were sealed by a home-made Teflon® holder. A Pt-sputtered Ti mesh and a saturated calomel electrode (SCE, Sigma–Aldrich) were used as a counter and reference electrode, respectively.

In order to remove dissolved oxygen from the electrolyte, N_2 purging was carried out at a rate of 50 cm^3 min^{-1} for 10 min before any electrochemical process was started. Electrochemical experiments including Ni electrodeposition and catalytic activity tests were controlled using a potentiostat (Autolab PGSTAT302, Metrohm). Linear sweep voltammetry (LSV) was employed to evaluate the potential range suitable for Ni electrodeposition on CPs; electrodeposition was then carried out using chronoamperometry (CA) involving variable deposition potential (E_{dep}) and deposition time (t_{dep}). The morphology and loading mass of the deposited Ni were characterized using field emission scanning electron microscopy (FESEM, S-4100, Hitachi) and inductively coupled plasma mass spectrometry (ICPMS, ELAN 6100 DRC Plus, PerkinElmer SCIEX), respectively. The catalytic activity of the Ni/CPs was evaluated using cyclic voltammetry (CV) at a scan rate of 50 mV s^{-1} in a 1.0 M KOH solution at room temperature.

The Ni/CPs were used for the fabrication of an AAEMWE. Fig. 1 shows a photograph of the cell configuration of the fabricated AAEMWE. The MEA (2 cm × 2 cm) was fabricated using a commercial AEM (A201, Tokuyama) sandwiched between two Ni/CPs. A graphite bipolar plate with serpentine channels (channel dimensions: 1.0 mm × 1.0 mm) provided the flow path for the reactants and products. The temperature of the cell was controlled using an external electric heater (50–70 °C). The cell was operated under constant current density controlled using a potentiostat (HCP 803, Bio-logic). The reactant (1.0 M KOH) was injected into the cathode by using a syringe pump at a feed rate of 1 mL min^{-1} and at a pre-heating temperature of 50 °C. The gas production rate was measured using a flow meter.

3. Results and discussion

The electrodes for the AAEMWE were fabricated using electrodeposition to form a Ni layer on the CP surface. The electrochemical behavior of Ni deposition on CP was studied using LSV, as shown in Fig. 2. The electrochemical reduction of Ni ions started at around −0.72 V (*vs.* SCE); the reduction current then gradually increased with a negatively increasing potential until a plateau was reached at −0.80 V, indicating the mass-transport limitation of Ni ions. The subsequent rapid increase in the current was due to the vigorous HER at the surface of the deposited Ni. On the other hand, in the absence of Ni ions, only a slight increase in the current originating at −0.90 V was observed, indicating a sluggish HER on bare CP. Using LSV, the deposition potential of Ni on CP was determined to be in the range from −0.75 to −1.15 V with intervals of 0.10 V at a constant deposition time of 50 s.

Fig. 3a shows CA curves for Ni electrodeposition at various deposition potentials. In the initial stages of CA, a drastic rise in the charging current for double layer capacitance, as well as Ni deposition current can be observed. Then, the currents decreased

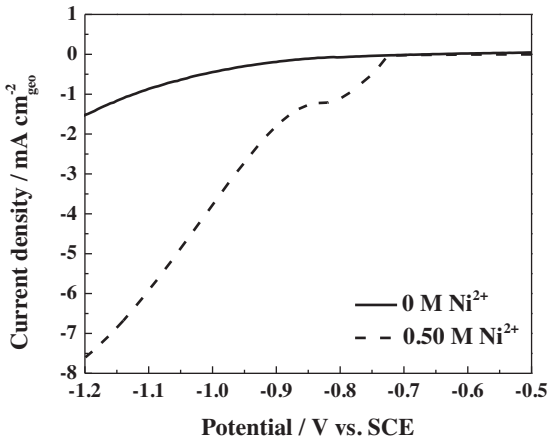

Fig. 2. LSV curves for CPs with/without 0.50 M of Ni^{2+} at a scan rate of 20 mV s^{-1}.

owing to charging current decay and Ni ion depletion in the electrodes; and, after several seconds, stabilized in combination with the onset of HER currents. The overall currents gradually increased with a negative shift in the deposition potential. The amount of deposited Ni was analyzed by ICPMS and its relation with the deposition potential is demonstrated in Fig. 3b. As shown in the figure, the Ni loading mass was proportional to the deposition potential with a sharp increase at −0.95 V. On the basis of CA and ICPMS results, the faradaic efficiencies for Ni deposition were calculated and are shown in Fig. 3b. At −0.75 V, the faradaic efficiency was 64.5%, indicating that a large proportion of the current was used for Ni deposition on CP. However, upon increasing the deposition potential, the faradaic efficiency significantly decreased to 30.0% at −0.85 V and to 14.5% at −1.15 V, owing to the evolution of a large amount of hydrogen. This result is in good agreement with the HER behavior during Ni deposition, as determined from the LSV analysis. For all Ni deposits, assuming a charge of 514 μC cm_{Ni}^{-2} for the formation of α-Ni(OH)$_2$ [32], electrochemical surface areas (ECSAs) were calculated from the peak area of an anodic CV sweep (−0.90 to −0.50 V) measured in 0.5 M NaOH at a scan rate of 10 mV s^{-1}, and the results are demonstrated in Fig. 3c. The roughness factors obtained by dividing the ECSA by the geometrical surface area (10.24 cm^2) are shown as a function of the deposition potential in Fig. 3d. The maximum roughness factor of 16.3 was obtained at a deposition potential of −0.95 V.

Fig. 4 shows the FESEM images of bare CP (Fig. 4a) and Ni/CPs (Fig. 4b–f) at varying deposition potentials with a fixed deposition time of 50 s. The morphologies of the deposited Ni varied with the deposition potential. At −0.75 V, a sparse population of isolated Ni

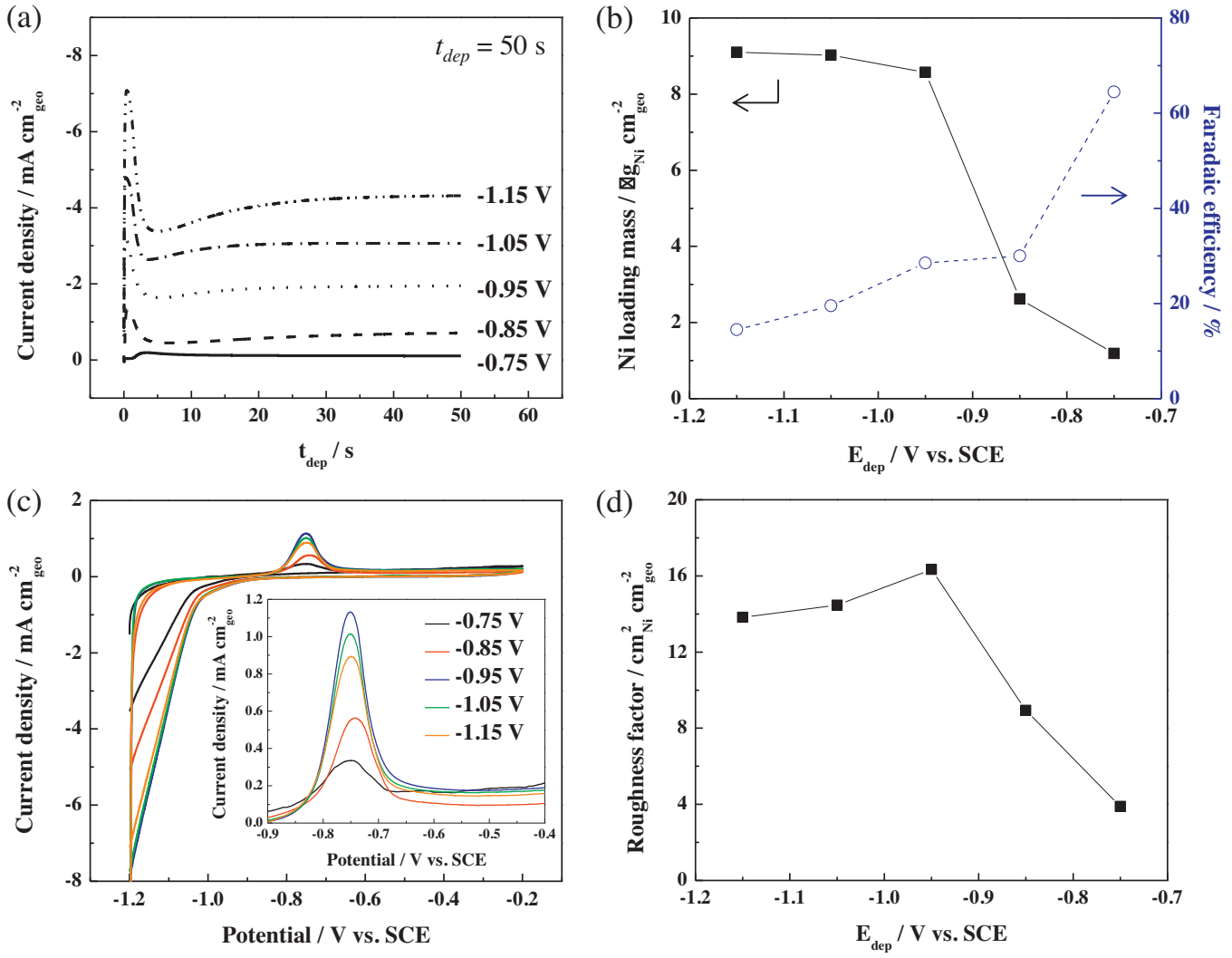

Fig. 3. (a) CA curves for Ni electrodeposition, (b) Ni loading mass and efficiency, (c) CV curves in 0.5 M NaOH at a scan rate of 10 mV s^{-1}, and (d) roughness factor, for various deposition potentials.

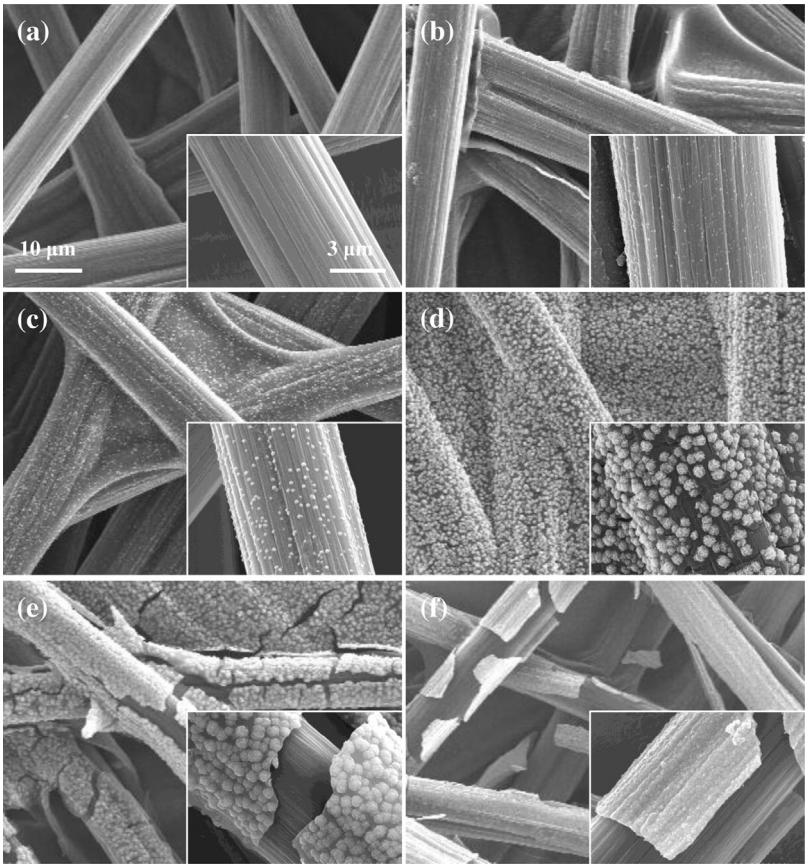

Fig. 4. FESEM images of (a) bare CP and Ni/CPs at (b) −0.75 V, (c) −0.85 V, (d) −0.95 V, (e) −1.05 V, and (f) −1.15 V for a constant deposition time of 50 s. The inset images show details at a high magnification.

particles was formed on the CP surface, as shown in Fig. 4b. On negatively increasing the deposition potential to −0.85 and −0.95 V, the Ni particles grew to sizes in the range from 170 nm to 630 nm (Fig. 4c–d). A further increase in the deposition potential to −1.05 and −1.15 V resulted in the formation of particle agglomerations and the emergence of film-like structures, as shown in Fig. 4e–f. This morphological change occurring upon varying the deposition potential is quite complex and can be explained in terms of various phenomena such as the number of nucleation sites, hydrogen gas adsorption during electrodeposition, and competition between translational and rotational diffusion [31,33]. At −1.05 and −1.15 V, the agglomerations of Ni particles were peeled off from CP fibers. This might be related to the building up of stresses on the deposited Ni owing to the increase in thickness, high curvature of CP fibers, and mechanical effect of generated hydrogen bubbles [34–36].

Electrochemical measurements were performed to evaluate the catalytic activities of Ni/CPs with respect to HER and OER in the KOH electrolyte. As shown in Fig. 5a, bare CP was found to be electrochemically inactive (black line) under the conditions and potential range employed in the present study. On the other hand, typical cyclic voltammograms corresponding to HER and OER behavior [37] were observed in case of Ni/CPs. First, HER started at around −1.05 V. Second, electrochemical redox reactions corresponding to the formation (anodic) and reduction (cathodic) of NiOOH [38] occurred in the potential range between 0 and 0.70 V. Then, upon the application of a more positive potential sweep, an OER current appeared that overlapped with the redox couple. To compare the catalytic activities of Ni/CPs that depended on the deposition potential, the current densities at −1.77 V for HER and at 0.86 V for OER, which correspond to an overpotential of 0.70 V in both cases, are shown in Fig. 5b. With a negative shift in the deposition potential from −0.75 to −0.95 V, the catalytic activities for both reactions gradually increased and showed a maximum at −0.95 V. However, a further increase in the deposition potential (−1.05 and −1.15 V) resulted in a decrease in the catalytic activity, presumably because the roughness factors of Ni started to decrease, as shown in Fig. 3d.

As indicated, the dependence of the catalytic activities of various Ni/CP combinations was in good accordance with the calculated roughness factors (Fig. 3d). This implies that the current densities for both HER and OER were affected mostly by the electrochemical surface area and not by any structural effects. In this regard, though the faradaic efficiency of Ni deposition was highest at a deposition potential of −0.75 V, this potential was not suitable for Ni catalyst formation since the roughness factor was the lowest owing to slow kinetics. Similarly, at high deposition potentials of −1.05 and −1.15 V, though the roughness factors were relatively high, the faradaic efficiencies were too low and a significant loss in the deposition current appeared at these potentials. Therefore, considering both the practical feasibility and activity of the electrodeposited Ni, it can be concluded that the optimum deposition potential in this study was −0.95 V, because of the reasonably high faradaic efficiency and excellent roughness factor (*i.e.*, highest activity) at this value.

At a deposition potential of −0.95 V, various deposition times were employed to achieve optimum Ni/CP deposition conditions for the preparation of AAEMWE. Fig. 6a demonstrates a CA curve for 300 s, showing similar features as observed in Fig. 3a. Fig. 6b shows the Ni loading amounts for various deposition times. The Ni loading amount rapidly increased with increasing deposition time from 1.0 $\mu g_{Ni}\ cm_{geo}^{-2}$ (5 s) to 9.8 $\mu g_{Ni}\ cm_{geo}^{-2}$ (60 s) and then further increased to 21.6 $\mu g_{Ni}\ cm_{geo}^{-2}$ at a slower rate until the

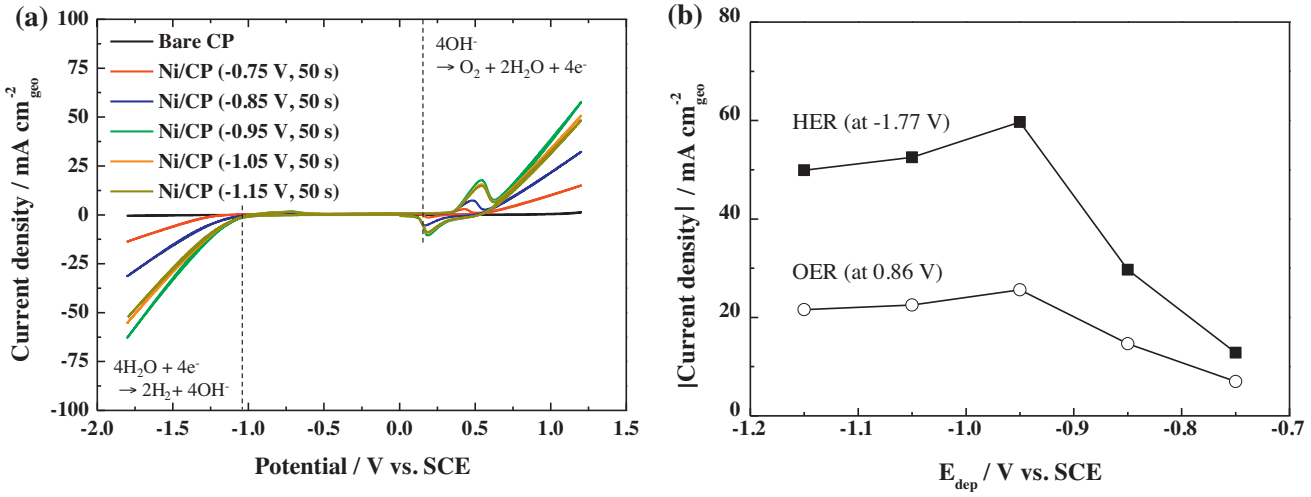

Fig. 5. (a) CV curves of bare CP and Ni/CPs in 1.0 M KOH at a scan rate of 50 mV s^{-1} at room temperature. (b) Recorded current densities for HER and OER at an overpotential of 0.70 V as a function of the deposition potential.

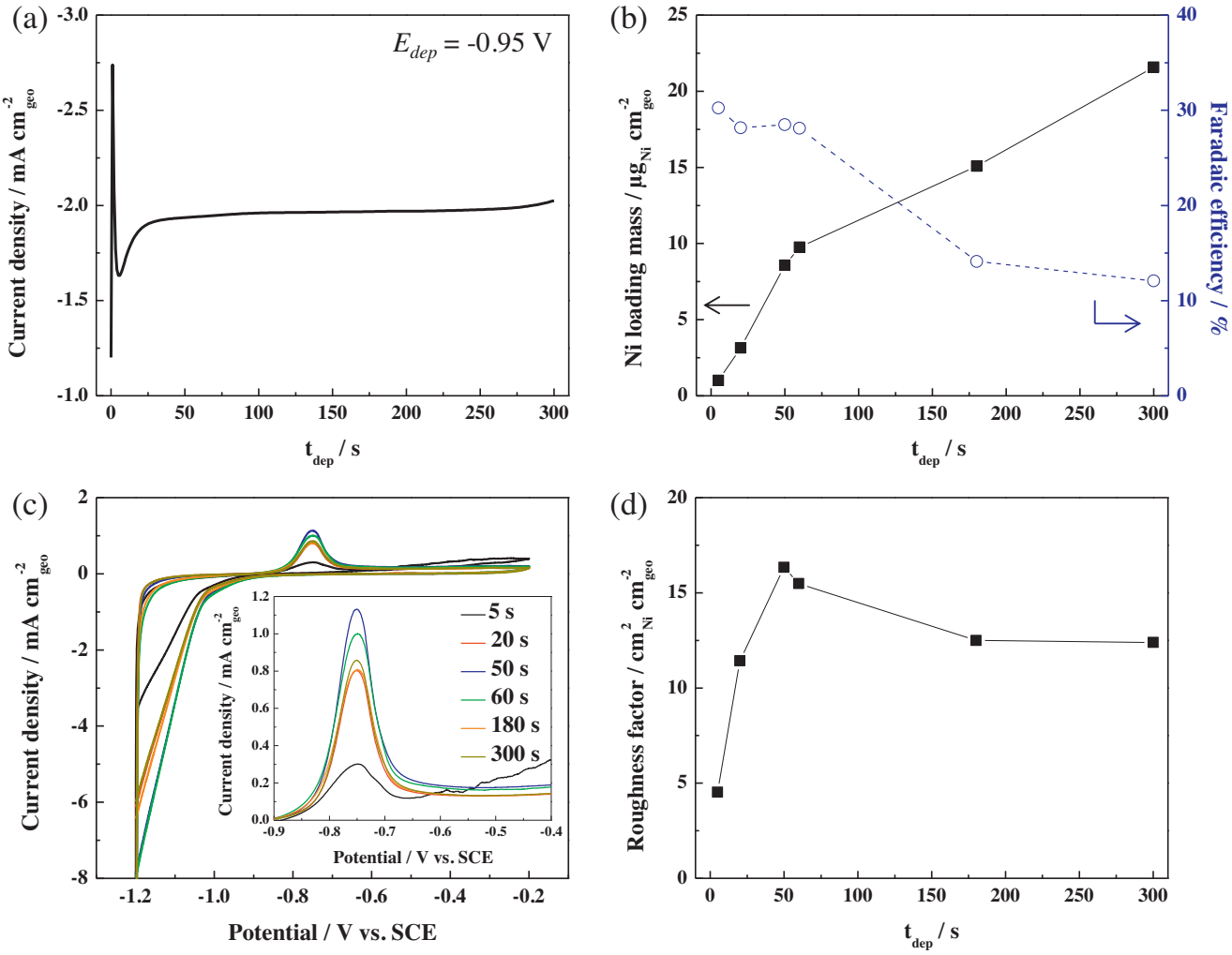

Fig. 6. (a) CA at −0.95 V for 300 s, (b) Ni loading mass and faradaic efficiency, (c) CV curves in 0.5 M NaOH at a scan rate of 10 mV s^{-1} and (d) roughness factor, for various deposition times.

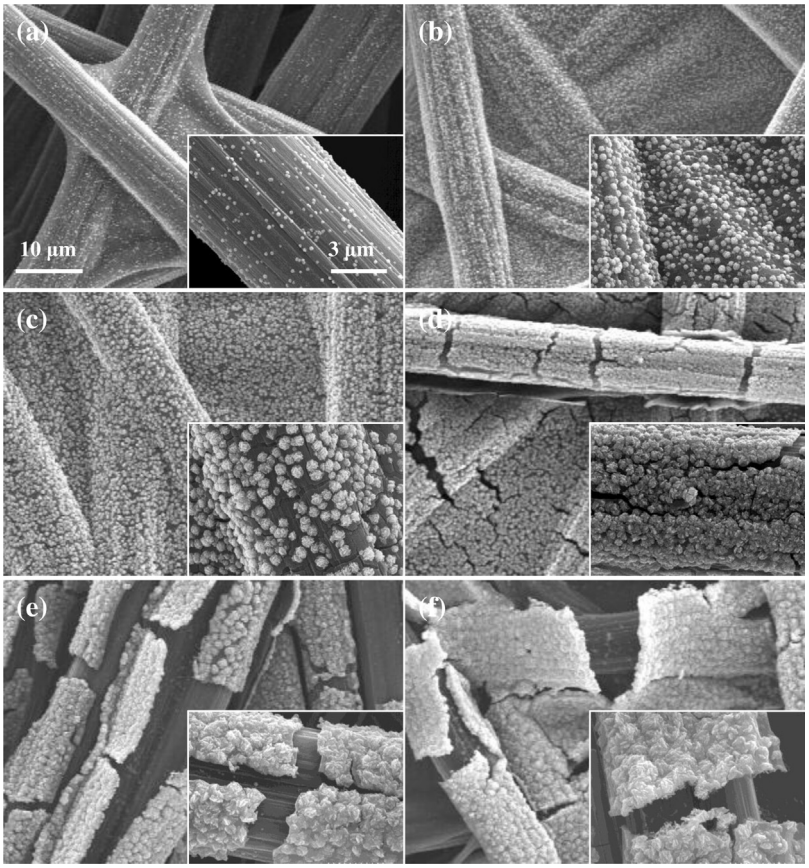

Fig. 7. FESEM images of Ni/CPs at (a) 5 s, (b) 20 s, (c) 50 s, (d) 60 s, (e) 180 s, and (f) 300 s at a constant deposition potential of -0.95 V. The inset images show details at a high magnification.

deposition time of 300 s was reached. The faradaic efficiency gradually decreased with time because of the insufficient mass transport of Ni^{2+} ions with increasing deposition time in combination with enhanced HER. The ECSAs of the prepared Ni/CPs were investigated by CV measurements in 0.5 M NaOH at a scan rate of 10 mV s^{-1} (Fig. 6c); further, the roughness factors were also calculated, and the results are shown in Fig. 6d. The highest roughness factor was observed at a deposition time of 50 s.

Fig. 7 shows the FESEM images of Ni/CPs for various deposition times. Isolated Ni particles were observed on the CP surface at a deposition time of 5 s, as shown in Fig. 7a. Such isolated Ni particles grew with increasing deposition time up to 50 s (Fig. 7b and c). Then, the agglomeration of Ni particles started at 60 s with the formation of several cracks on the deposited Ni film (Fig. 7d). With the increase in deposition time to 180 and 300 s, the agglomerations of Ni particles peeled off from the CP surface (Fig. 7e–f), which might

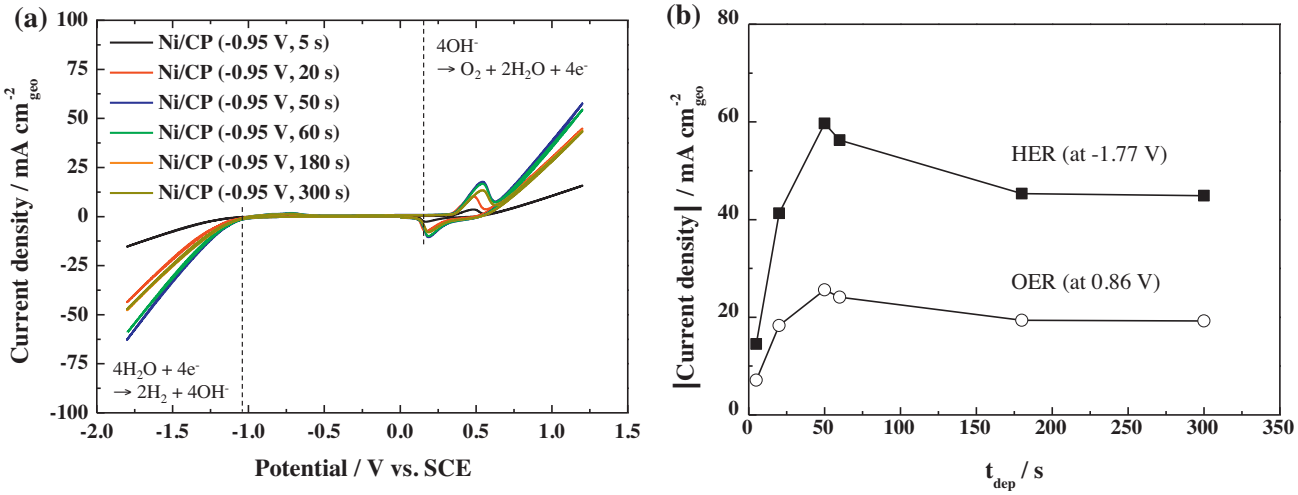

Fig. 8. (a) CV curves for Ni/CPs in 1.0 M KOH at a scan rate of 50 mV s^{-1} at room temperature. (b) Recorded current densities for HER and OER at an overpotential of 0.70 V as a function of deposition time.

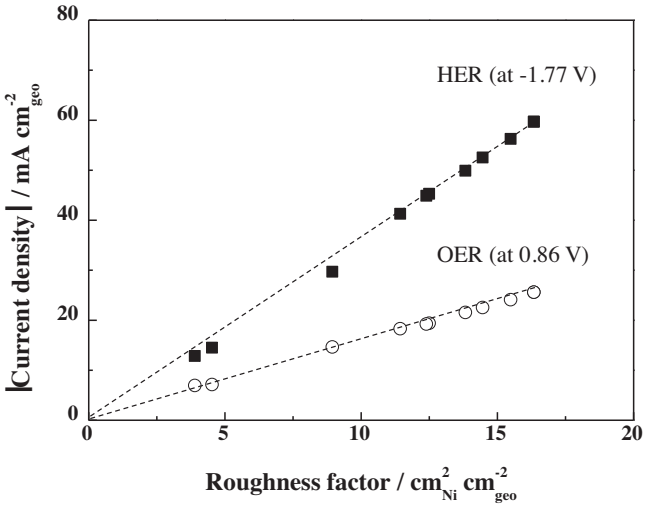

Fig. 9. Recorded current densities from CVs for both HER and OER at an overpotential of 0.70 V as a function of roughness factor.

have been induced by expansive stress on deposited Ni, as observed in Fig. 3e and f. The results of the FESEM analysis agreed well with the Ni loading mass and roughness factor.

The catalytic activities of Ni/CPs at various deposition times were evaluated by CV measurements in 1.0 M KOH at a scan rate of 50 mV s^{-1}, and the results are demonstrated in Fig. 8a. The current densities for both HER and OER were determined from cyclic voltammograms at fixed potentials (−1.77 V for HER and 0.86 V for OER), and the results are summarized in Fig. 8b. The current densities for both reactions increased with an increase in the deposition time from 5 to 50 s. This is in good agreement with the tendency shown by roughness factors (Fig. 6d). The highest current density was observed at a Ni deposition time of 50 s after which the values decreased slightly owing to the agglomerated morphology corresponding to a decrease in the roughness factor. Fig. 9 shows a summary of the relationship between the roughness factors and catalytic activities for both HER and OER. Data points were collected from different Ni/CP samples prepared by employing various deposition potentials and times. The catalytic activities of Ni/CPs with respect to both HER and OER showed linear relationships with the roughness factors. It is clear that the roughness factor, which is proportional to the ECSA, was the dominant factor determining the catalytic activities.

Fig. 10a shows a polarization curve for the AAEMWE equipped with Ni/CP (−0.95 V for 50 s), obtained for various cell compression pressures. It should be noted that no ionomer was used for AAEMWE fabrication in this study. The cell was compressed by applying pressures of 3.5, 4.1, 4.8, and 5.5 MPa, generated by screws, as shown in Fig. 1. The operating temperature and feed rate were 50 °C and 1 mL min^{-1} (1.0 M KOH), respectively. Each point in the polarization curve was recorded after 1 min of stabilization using chronopotentiometry. In the initial stage (low current density region below 20 mA cm^{-2}), the cell voltage decreased with increasing screw pressure because the contact between the membrane and catalyst might have improved at a high screw pressure. However, with increasing current density (above 20 mA cm^{-2}), the opposite behavior was observed at pressures of 4.1, 4.8, and 5.5 MPa. The cell showed the lowest performance at 3.5 MPa for all current density values owing to poor contact. At a highest screw pressure (5.5 MPa), the cell voltage rapidly increased with the current density. This could be due to the poor transport of generated hydrogen and oxygen bubbles, induced by a severely compressed CP. Thus, the use of a highly compressed CP could not provide sufficient pathways for the gases to be exhausted. The bubbles remaining in the cell decreased the cell performance by covering the active sites of the catalyst. Some reports in the literature have already mentioned a large overpotential resulting from the gas generated on the catalyst surface during electrolysis [39,40]. With decreasing pressure, the gas bubbles were relieved owing to an improvement in gas exhaust. In this regard, the highest cell performance was obtained at a pressure of 4.1 MPa, thus indicating the optimal screw pressure in terms of the contact between the membrane and Ni/CP, as well as with respect to the gas transport in the system.

Fig. 10b shows the effect of operating temperature on the cell performance at a pressure of 4.1 MPa. The cell performance gradually increased with an increase in the operating temperature from 50 to 70 °C. At a cell voltage of 1.6 V, when the cell was mostly free from gas transport restrictions, the activation energy for alkaline water electrolysis was calculated from an Arrhenius plot. From the relationship between the logarithm of the current density and reciprocal temperature, the activation energy in the present study was determined to be approximately 12 kcal mol^{-1}. This value is in good agreement with that reported by Srinivasan et al. (15 kcal mol^{-1}) [41]. Though it is still very difficult to provide a plausible interpretation, an increase of about 87% in the cell

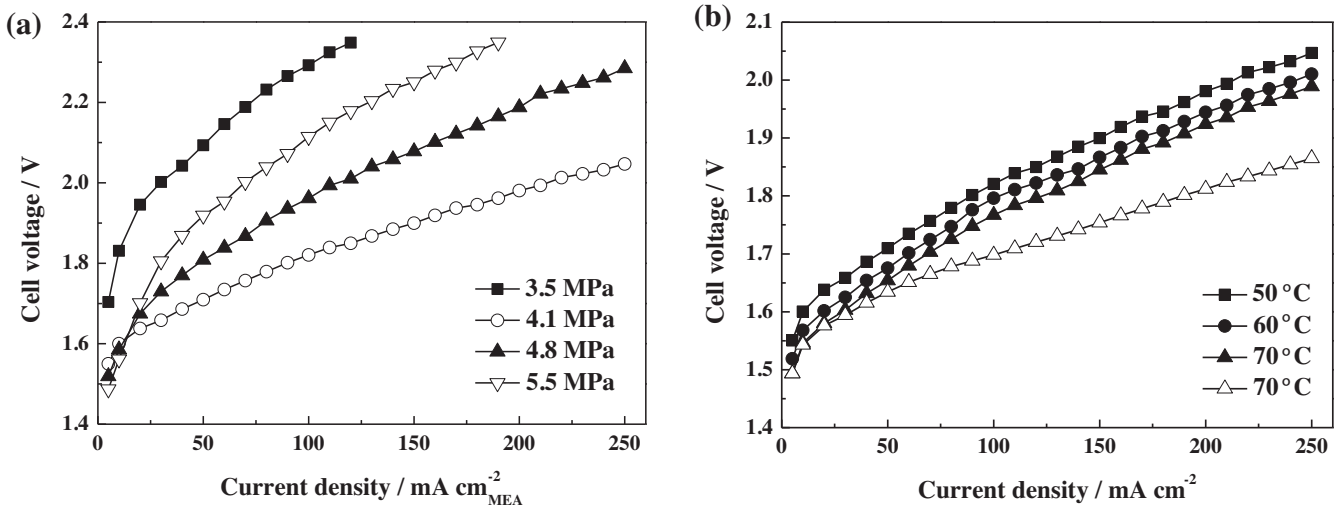

Fig. 10. Polarization curves for AAEMWE at a feed rate of 1 mL min^{-1} (1.0 M KOH) (a) at 50 °C, for various MEA compression pressures and (b) at a MEA compression pressure of 4.1 MPa, for various operating temperatures (solid: with cathodic flow only, open: with cathodic and anodic flows).

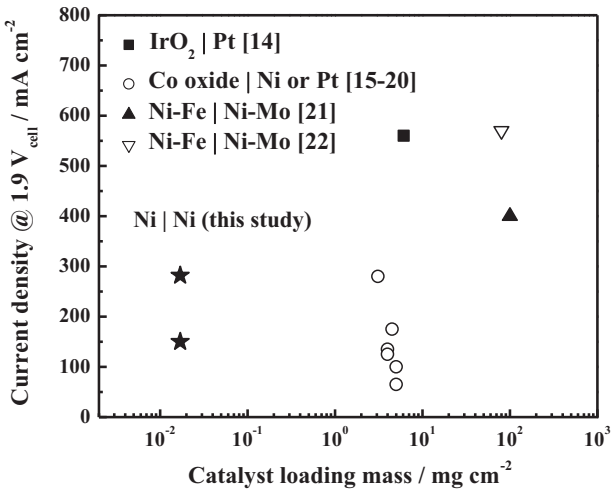

Fig. 11. Performance of AAEMWE fabricated in this study and comparison of results obtained with those reported in the literature (solid: KOH feed, open: D. I. water feed) [14–22]. Used anode and cathode catalysts were indicated in legends.

performance was observed at 1.9 V when the KOH solution was injected to both electrodes at an operating temperature of 70 °C (open triangle, Fig. 10(b)). Complex phenomena such as the removal of bubbles by the extra flow of KOH and increase in conductivity through AEM, as well as other effects within the catalyst structures may be responsible for the observed increase in cell performance.

Fig. 11 demonstrates a comparison between literature results for AAEMWE performance characterized by the current density at 1.9 V and the catalyst loading mass and the results obtained in this study. For the performance of an MEA containing noble metal catalysts (CCM method), Wang et al. demonstrated a high current density of 560 mA cm^{-2} by using large amounts of Pt (3.2 mg cm^{-2}) and IrO_2 (2.9 mg cm^{-2}), which are noble, with a 1.0 M KOH feed [14]. On the other hand, Scott and group used transition metals ($\leq$3.0 mg cm^{-2}) as catalysts for OER along with a deionized water feed; they obtained a maximum current density of 280 mA cm^{-2} by employing $Cu_{0.6}Mn_{0.3}Co_{2.1}O_4$ as a catalyst [15–20]. Compared with these results, when huge amounts of transition metal alloy catalysts (Ni–Mo and Ni–Fe) were loaded in an MEA (up to 100 mg cm^{-2}) with a highly concentrated KOH feed (5 M), the cell showed an enhanced current density of 400 mA cm^{-2}, as reported by Villa and his colleagues [21]. However, the current density was still lower than that obtained using a MEA containing a noble metal catalyst. In particular, Zhuang et al. demonstrated a comparably high current density of 570 mA cm^{-2} by using a Ni-alloy catalyst even though they used a deionized water feed [22]. However, the catalyst amount was still very high at ~80 mg cm^{-2}. Additionally, in the case of bulk Ni electrodes, for example in form of Ni foam [23] or plates [24], lower current densities of 120 mA cm^{-2} were obtained, as reported by Bouzek et al. and Aili et al. This is because bulk electrodes are not suitable for high catalyst utilization. In the present study, the electrodeposited Ni on CPs showed current densities of 150 and 280 mA cm^{-2} with cathodic and cathodic/anodic 1.0 M KOH flows, respectively, by using extremely low amounts of Ni (17.0 μg_{Ni} cm^{-2} for both electrodes and 8.5 μg_{Ni} cm^{-2} for each electrode) in the MEA. The results presented herein demonstrate a promising possibility for the preparation of AAEMWE electrodes by means of electrodeposition.

4. Conclusions

An MEA with Ni/CP electrodes was fabricated for use in an AAEMWE by direct electrodepositon of Ni on CPs. Considering the roughness factor of Ni and the faradaic efficiency during electrodeposition, the optimized Ni/CP electrode was obtained under the deposition conditions of −0.95 V and 50 s. Under these conditions, the fabricated Ni/CP electrode exhibited current densities of −59.7 mA cm^{-2} for HER and 25.6 mA cm^{-2} for OER in half-cell tests at an overpotential of 0.70 V for each reaction. The single cell test at various cell compression pressures suggested that the removal of trapped bubbles can be an important factor in improving electrolysis performances. The MEA made of Ni/CP electrodes with a Ni amount of 17.0 μg_{Ni} cm^{-2} demonstrated a current density of 150 mA cm^{-2} at a cell voltage of 1.9 V under an operating temperature of 50 °C. These results suggest that electrodeposition is a highly effective technique for the fabrication of AAEMWE electrodes with an extremely low catalyst loading. As a future work, the long-term operation of AAEMWEs fabricated using the proposed method should be investigated to verify the stability of Ni/CP electrodes.

Acknowledgement

This work was supported by the Korea CCS R&D Center (KCRC) grant funded by the Korea Government (Ministry of Science, ICT & Future Planning) (No. 2013M1A8A1038315).

References

[1] P. Barbaro, C. Bianchini, Catalysis for Sustainable Energy Production, Wiley-VCH, Weinheim, 2009.
[2] J.A. Turner, Science 305 (2004) 972–974.
[3] K. Christopher, R. Dimitrios, Energy Environ. Sci. 5 (2012) 6640–6651.
[4] J.D. Holladay, J. Hu, D.L. King, Y. Wang, Catal. Today 139 (2009) 244–260.
[5] G. Schiller, R. Henne, P. Mohr, V. Peinecke, Int. J. Hydrogen Energy 23 (1998) 761–765.
[6] K. Zeng, D. Zhang, Prog. Energy Combust. 36 (2010) 307–326.
[7] S. Marini, P. Salvi, P. Nelli, R. Pesenti, M. Villa, M. Berrettoni, G. Zangari, Y. Kiros, Electrochim. Acta 82 (2012) 384–391.
[8] A.S. Aricò, S. Siracusano, N. Briguglio, V. Baglio, A.D. Blasi, V. Antonucci, J. Appl. Electrochem. 43 (2013) 107–118.
[9] S.A. Grigoriev, V.I. Porembsky, V.N. Fateev, Int. J. Hydrogen Energy 31 (2006) 171–175.
[10] A. Goñi-Urtiaga, D. Presvytes, K. Scott, Int. J. Hydrogen Energy 37 (2012) 3358–3372.
[11] H. Ito, T. Maeda, A. Nakano, H. Takenaka, Int. J. Hydrogen Energy 36 (2011) 10527–10540.
[12] E. Slavcheva, I. Radev, S. Bliznakov, G. Topalov, P. Andreev, E. Budevski, Electrochim. Acta 52 (2007) 3889–3894.
[13] S. Song, H. Zhang, X. Ma, Z. Shao, R.T. Baker, B. Yi, Int. J. Hydrogen Energy 33 (2008) 4955–4961.
[14] Y. Leng, G. Chen, A.J. Mendoza, T.B. Tighe, M.A. Hickner, C. Wang, J. Am. Chem. Soc. 134 (2012) 9054–9057.
[15] Y. Cao, X. Wu, K. Scott, Int. J. Hydrogen Energy 37 (2012) 9524–9528.
[16] X. Wu, K. Scott, J. Power Sources 214 (2012) 124–129.
[17] X. Wu, K. Scott, J. Mater. Chem. 21 (2011) 12344–12351.
[18] X. Wu, K. Scott, J. Power Sources 206 (2012) 14–19.
[19] X. Wu, K. Scott, Int. J. Hydrogen Energy 38 (2013) 3123–3129.
[20] X. Wu, K. Scott, F. Xie, N. Alford, J. Power Sources 246 (2014) 225–231.
[21] P. Salvi, P. Nelli, M. Villa, Y. Kiros, G. Zangari, G. Bruni, A. Marini, C. Milanese, Int. J. Hydrogen Energy 36 (2011) 7816–7821.
[22] L. Xiao, S. Zhang, J. Pan, C. Yang, M. He, L. Zhuang, J. Lu, Energy Environ. Sci. 5 (2012) 7869–7871.
[23] J. Hnát, M. Paidar, J. Schauer, J. Žitka, K. Bouzek, J. Appl. Electrochem. 42 (2012) 545–554.
[24] D. Aili, M.K. Hansen, R.F. Renzaho, Q. Li, E. Christensen, J.O. Jensen, N.J. Bjerrum, J. Membr. Sci. 447 (2013) 424–432.
[25] G. Merle, M. Wessling, K. Nijmeijer, J. Membr. Sci. 377 (2011) 1–35.
[26] J.R. Varcoe, R.C.T. Slade, Fuel Cells 5 (2005) 187–200.
[27] K. Shen, J. Pang, S. Feng, Y. Wang, Z. Jiang, J. Membr. Sci. 440 (2013) 20–28.
[28] J. Qiao, J. Zhang, J. Zhang, J. Power Sources 237 (2013) 1–4.
[29] M. Piana, M. Boccia, A. Filpi, E. Flammia, H.A. Miller, M. Orsini, F. Salusti, S. Santiccioli, F. Ciardelli, A. Pucci, J. Power Sources 195 (2010) 5875–5881.
[30] S.H. Ahn, S. Jeon, H. Park, S. Kim, H. Kim, E. Cho, D. Henkensmeier, S.J. Yoo, S.W. Nam, T. Lim, J.H. Jang, Int. J. Hydrogen Energy 38 (2013) 9826–9834.
[31] S.H. Ahn, S.J. Hwang, S.J. Yoo, I. Choi, H. Kim, J.H. Jang, S.W. Nam, T. Lim, T. Lim, S. Kim, J.J. Kim, J. Mater. Chem. 22 (2012) 15153–15159.
[32] S.A.S. Machado, L.A. Avaca, Electrochim. Acta 39 (1994) 1385–1391.
[33] L. Gránásy, T. Pusztai, T. Börzsönyi, J.A. Warren, J.F. Douglas, Nat. Mater. 3 (2004) 645–650.
[34] M. Sánchez, J. Rams, A. Ureña, Oxid. Met. 69 (2008) 327–341.

[35] B.R. Powell Jr., G.E. Youngblood, D.P.H. Hasselman, L.D. Bentsen, J. Am. Ceram. Soc. 63 (1980) 581–586.
[36] K. Nielsch, F. Müller, A. Li, U. Gösele, Adv. Mater. 12 (2000) 582–586.
[37] D.A. Corrigan, R.M. Bendert, J. Electrochem. Soc. 136 (1989) 723–728.
[38] P. Oliva, J. Leonardi, J.F. Laurent, C. Delmas, J.J. Braconnier, M. Figlarz, F. Fievet, A. de Guibert, J. Power Sources 8 (1982) 229–255.
[39] S.H. Ahn, I. Choi, H. Park, S.J. Hwang, S.J. Yoo, E. Cho, H. Kim, D. Henkensmeier, S.W. Nam, S. Kim, J.H. Jang, Chem. Commun. 49 (2013) 9323–9325.
[40] D. Zhang, K. Zeng, Ind. Eng. Chem. Res. 51 (2012) 13825–13832.
[41] M.H. Miles, G. Kissel, P.W.T. Lu, S. Srinivasan, J. Electrochem. Soc. 123 (1976) 332–336.